

# DEIR: Efficient and Robust Exploration through Discriminative-Model-Based Episodic Intrinsic Rewards

Shanchuan Wan<sup>1</sup>, Yujin Tang<sup>2</sup>, Yingtao Tian<sup>2</sup> and Tomoyuki Kaneko<sup>1</sup>

<sup>1</sup>The University of Tokyo

<sup>2</sup>Google Research, Brain Team

swan@game.c.u-tokyo.ac.jp, {yujintang, alantian}@google.com, kaneko@graco.c.u-tokyo.ac.jp

## Abstract

Exploration is a fundamental aspect of reinforcement learning (RL), and its effectiveness crucially decides the performance of RL algorithms, especially when facing sparse extrinsic rewards. Recent studies showed the effectiveness of encouraging exploration with intrinsic rewards estimated from novelty in observations. However, there is a gap between the novelty of an observation and an exploration in general, because the stochasticity in the environment as well as the behavior of an agent may affect the observation. To estimate exploratory behaviors accurately, we propose **DEIR**, a novel method where we theoretically derive an intrinsic reward from a conditional mutual information term that principally scales with the novelty contributed by agent explorations, and materialize the reward with a discriminative forward model. We conduct extensive experiments in both standard and hardened exploration games in MiniGrid to show that DEIR quickly learns a better policy than baselines. Our evaluations in ProcGen demonstrate both generalization capabilities and the general applicability of our intrinsic reward.

## 1 Introduction

Exploration is an important aspect of reinforcement learning (RL), as suggested by the famous exploration-exploitation trade-off [Sutton and Barto, 2018]: Overall, the agent that only exploits with the current policy would be stuck and fail to improve its policy any more due to the lack of novel experiences. Effective exploration is non-trivial, especially in those tasks where environmental rewards are sparse. Relying on unstructured exploration (e.g.,  $\epsilon$ -greedy, randomized probability matching) requires exponential number of samples and is unlikely to achieve a satisfactory level of exploration. On the other hand, manually designing dense rewards with domain knowledge addresses this issue with promising results in several aspects where RL has significantly progressed such as game playing and robotics [Mnih *et al.*, 2015; Baker *et al.*, 2019; Hafner *et al.*, 2020]. However, given that the huge amount of knowledge and effort are required, designing such dense rewards is only feasible in a handful of tasks, thus leaving effective exploration challenging still.

To tackle this issue, several works proposed to guide the exploration with intrinsic rewards, or rewards that are internal to agents, including ICM [Pathak *et al.*, 2017], RND [Burda *et al.*, 2019], NGU [Badia *et al.*, 2020] and NovelD [Zhang *et al.*, 2021]. In these works, the intrinsic reward is devised to encourage visiting states that are likely to be more novel,

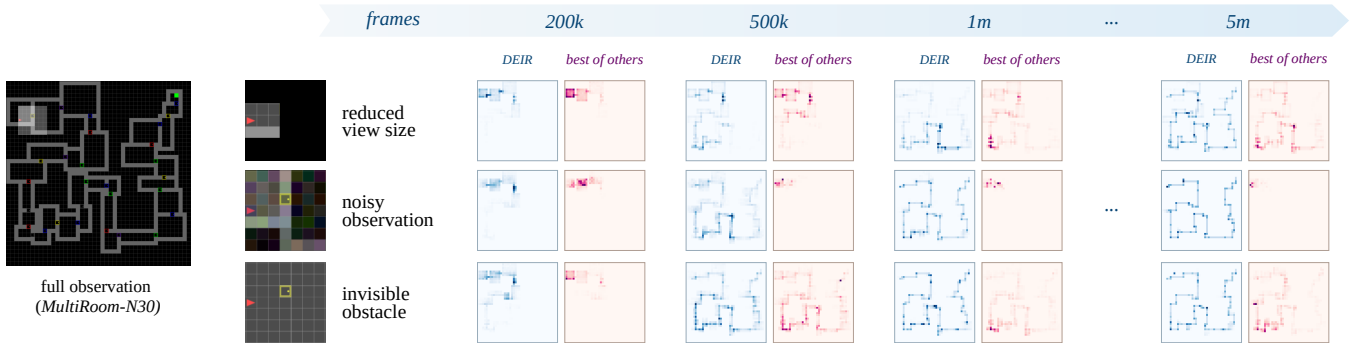


Figure 1: Enlarged *MultiRoom* environment (the leftmost figure) from MiniGrid with 30 cascaded rooms as a representative of environments with sparse extrinsic rewards, where the agent (the upper left red dot) is tasked with finding the optimal path to the goal (the upper right green dot). We create hardened variants (the three rows on the right) with extra difficulties, such as reduced view sizes, noisy observations, and invisible obstacles. In those challenging tasks, existing methods (ICM, RND, NGU and NovelD) fail to or require a prohibitive number of episodes to find an optimal path. In contrast, our proposed DEIR leveraging a mutual information based intrinsic reward and a contrastive learning inspired model, is capable of diverse exploration and significantly better performances. More discussions are in Section 4.2.

where novelty is defined either as the distance between the current and past observations or as the surprise from model predictions and realities. These works show encouraging empirical results in better exploration efficiency, but the relationship between the observed novelty and the agent’s actions has not been explicitly decoupled yet. Here, effectively handling trivial novelties remains unaddressed, since they are rooted from the stochasticity in the environment’s dynamics and have few to do with the agent’s exploration capabilities (e.g., the “noisy TV” problem [Pathak *et al.*, 2017]).

In this paper, we fill in this blank with **DEIR**, or **Discriminative-model-based Episodic Intrinsic Reward**, a novel intrinsic reward design that considers not only the observed novelty, but also the effective contribution brought by the agent. In DEIR, we theoretically derive an intrinsic reward by scaling the novelty metric with a conditional mutual information between the observation distances and the agent’s actions, and developed the intrinsic reward with a simple formula serving as the lower bound of our objective. Thus DEIR is designed to distinguish the contribution to novelties caused by state transitions and that by the agent’s policy. To materialize the computation of proposed reward, we devise a discriminative forward model that jointly learns the environment’s dynamics and the discrimination of genuine and fake trajectories. To show the effectiveness of our method, we evaluate DEIR in both standard and hardened MiniGrid [Chevalier-Boisvert *et al.*, 2018] tasks (grid-world exploration games where no reward is given until reaching the goal). DEIR outperforms existing methods on both the standard and the hardened settings, where the baseline methods sometimes fail to learn at all (see Figure 1). To confirm DEIR’s generalization capability in tasks with higher dimensional observations, we also conducted experiments in ProcGen [Cobbe *et al.*, 2020] (video games with randomly procedurally-generated levels that require planning, manipulation, or exploration), and DEIR demonstrated state-of-the-art performances in the tasks. Finally, we include in-depth analysis of our method in experiments to help better understand its behavior.

Our contributions can be summarized as: (1) our method, theoretically grounded, effectively decouples the stochasticity in the environment and the novel states realized by an agent’s exploratory action. (2) Our method empirically outperforms the best of others in this line of work by a large margin, especially in hardened MiniGrid tasks, but not limited thereto. DEIR could also apply to a variety of tasks.

## 2 Related Work

Curiosity-driven exploration is widely studied in RL literatures, works on this topic generally fall into two categories: *Novelty driven methods* that seek for novel agent observations, and *Prediction error driven methods* that are motivated by surprises between predictions and realities.

**Novelty driven methods** generally define a distance metric between pairs of observations, and then formulate this distance as intrinsic rewards to encourage more exploration in RL roll-outs. Among early works, count-based methods keep record of how many times distinct states are vis-

ited, and use that count differences as intrinsic rewards [Li, 2017]. Simple as they are, count-based methods have difficulties in tasks with continuous states or high-dimensional observations. To overcome this problem, neural networks are introduced to encode the states and observation. For example, RND [Burda *et al.*, 2019] measures the distance as the difference between outputs of a randomly initialized neural network and a parameter-fixed target neural network. In this work another network is used to distill the former network into the latter one, effectively “evolving” a distance metric that adjusts dynamically with the agent’s experience. Most recently, NovelD [Zhang *et al.*, 2021] proposed that RND is applied to evaluate the distances between pairs of observations, and a boundary between explored and unexplored regions is encountered when the distance is larger than a pre-defined threshold, and large intrinsic rewards are provided when the agent crosses boundaries. In this way, NovelD encourages the agent to explore in a manner similar to breadth-first search and has demonstrated so far state-of-the-art performance on many MiniGrid tasks. In practice, measuring novelty often requires analysis of the distribution of the environmental states. Even so, “noisy TV”-like problems can still occur where novelty in the observation space is purely due to the stochasticity in environment’s dynamics and prevents the agent from meaningful explorations.

**Prediction error driven methods**, in contrast, learn a model of the environment’s dynamics and with which they make predictions for future states. Large deviations between the predictions and the realities suggest regimes where the model is insufficiently learned. Intrinsic rewards, positively correlated to prediction errors, encourage the agent to explore more in those states. One of the representative works in this category is ICM [Pathak *et al.*, 2017], which jointly trains both the forward and the inverse transition models to better capture the environment’s dynamics, but only uses the forward model’s predictions error to generate intrinsic rewards for the agent. Similarly, Never-Give-Up (NGU) [Badia *et al.*, 2020] introduces the inverse model from ICM in its episodic intrinsic reward generation module. Their final intrinsic reward is based on the Euclidean distances of the K-nearest embeddings of the recently visited states. Prediction error driven methods requires approximating the environment’s dynamics with neural networks, which is especially hard in high-dimensional spaces. Still, as demonstrated by ICM, training with auxiliary tasks seems to be worthwhile efforts.

Our method can be regarded as a combination of the two categories: While we explicitly encourage our agent to seek for novel observations, we also rely on a discriminative model to construct a conditional mutual information term that scales the novelty in the observation space, hence incorporating prediction error driven methods implicitly. Unlike conventional novelty-driven method, our conditional mutual information scaling effectively eliminates the novelties rooted in the environment’s stochasticity other than those brought by the agent’s explorations and has granted us better performances (see Figure 1). To illustrate the difference from existing prediction error driven method, our model learns both the environment’s dynamics and the capability to tell the genuine and fake trajectories apart. Consistent with the results reported in

the line of contrastive learning studies [Laskin *et al.*, 2020; Agarwal *et al.*, 2021], the discriminative nature of our model encodes the observations in a space closely related to the underlying tasks and allows us to measure the distances between observations more accurately. Furthermore, we employ a recurrent neural network in our discriminative model to capture temporal features.

### 3 Proposed Method

#### 3.1 Background and Notations

A Markov Decision Process (MDP) [Sutton and Barto, 2018] can be defined as a tuple  $(S, A, r, f, P_0, \gamma)$ , where  $S$  is the state space,  $A$  is the action space,  $r(s_t, a_t, s_{t+1})$  is the reward function,  $f(s_t, a_t)$  is the environmental transition function,  $P_0$  is the distribution of the initial state  $s_0$ , and  $\gamma \in [0, 1]$  is the reward discount factor. The goal is to optimize a policy  $\pi : S \times A \rightarrow \mathbb{R}$  so that the expected accumulated reward  $\mathbb{E}_{s_0 \sim P_0} [\sum_t \gamma^t r(s_t, a_t, s_{t+1})]$  is maximized. However, in a partially observable MDP (POMDP)  $s_t \in S$  is not accessible to the agent. A common practice is to use instead  $\pi(a_t | \tau_t)$  for policy, where  $\tau_t = \{o_0, o_1, \dots, o_t\}$  is an approximation of  $s_t$ , and in many works realized by recurrent neural networks (RNN) to best utilize available historical information.

Following popular studies, we define the reward function to be the weighted sum of extrinsic (those from the environment) and intrinsic (those from curiosity) rewards:  $r(s_t, a_t, s_{t+1}) = r_t^E + \beta \cdot r_t^I$ , where  $r_t^E$  and  $r_t^I$  (both functions of  $(s_t, a_t, s_{t+1})$ ) are respectively the extrinsic and intrinsic rewards at time step  $t$ , and  $\beta$  is a hyperparameter.

#### 3.2 Episodic Intrinsic Reward

##### Scaling the Novelty

For a pair of states  $(s_t, s_i), i \in [0, t)$  and the action  $a_t$ , we want a novel state (valuable for exploration) to have a large distance between observations  $(o_{t+1}, o_i)$ , where the distance is also closely related to the action  $a_t$ . Intuitively, it is crucial to distinguish a stochastic transition inherent in an environment and a transition realized by an exploratory action by the agent. This leads to our primary objective to be maximized

$$J = \text{dist}(o_{t+1}, o_i) \cdot I(\text{dist}(o_{t+1}, o_i); a_t | s_t, s_i)$$

as a product of the distance  $\text{dist}(o_{t+1}, o_i)$  (denoted as  $D_{t+1,i}$ ) between observations and conditional mutual information

$$I(D_{t+1,i}; a_t | s_t, s_i) = \mathbb{E}_{s_t, s_i, a_t} [\text{D}_{\text{KL}}(p(D_{t+1,i} | a_t, s_t, s_i) \| p(D_{t+1,i} | s_t, s_i))].$$

With Bretagnolle–Huber inequality, we have

$$\text{D}_{\text{KL}}(P \| Q) \geq -\log(1 - d_{\text{TV}}^2(P, Q))$$

where we denote  $P(x) = p(x | a_t, s_t, s_i)$  and  $Q(x) = p(x | s_t, s_i)$ , and  $d_{\text{TV}}(P, Q) = \frac{1}{2} \|P - Q\|_1$  is the total variation between  $P$  and  $Q$ .

Furthermore, we notice in deterministic environments (including partially observable cases) that (a)  $P$  is a unit impulse function which has the only non-zero value at  $D_{t+1,i}$ , and (b) we can assume the  $D_{t+1,i} | s_t, s_i \sim \text{Exp}(\lambda = 1/\text{dist}(s_t, s_i))$  to match the distance between observations and that of their

underlying states. Thus we devise a simplified surrogate function for the mutual information:

$$\text{D}_{\text{KL}}(P \| Q) \geq \log(\text{dist}(s_t, s_i)) + \frac{\text{dist}(o_{t+1}, o_i)}{\text{dist}(s_t, s_i)} + \text{const.}$$

Substituting it back to the objective, we have

$$J \geq \text{dist}(o_{t+1}, o_i) \cdot$$

$$\mathbb{E}_{s_t, s_i, a_t} \left( \log(\text{dist}(s_t, s_i)) + \frac{\text{dist}(o_{t+1}, o_i)}{\text{dist}(s_t, s_i)} \right). \quad (1)$$

To make it tractable, we simplify the right hand side more and have

$$J \geq \min_i \frac{\text{dist}^2(o_{t+1}, o_i)}{\text{dist}(s_t, s_i)}, \quad (2)$$

which is a lower bound for the original objective. It is simpler and empirically performs as well as or even better than Equation 1. We speculate that the improvement in minimum value is crucial to improve the expectation value. Detailed derivation can be found in Appendix A.1.

#### Intrinsic Reward Design

To maximize our objective through the lower bound in Equation 2, we propose our intrinsic reward in an episodic manner:

$$r_t^I = \min_{\forall i \in [0, t)} \left\{ \frac{\text{dist}^2(e_i^{\text{OBS}}, e_{t+1}^{\text{OBS}})}{\text{dist}(e_i^{\text{TRAJ}}, e_t^{\text{TRAJ}}) + \epsilon} \right\}, \quad (3)$$

where  $e_t^{\text{OBS}}$  is the embedding of observation  $o_t$ ,  $e_t^{\text{TRAJ}}$  is the embedding of trajectory  $\tau_t$  at time step  $t$  in an episode,  $\text{dist}$  is the Euclidean distance between two embeddings, and  $\epsilon$  is a small constant ( $= 10^{-6}$  in our experiments) for numeric stability. Note that in partially observable environments the full information regarding  $s_t$  is inaccessible,  $e_t^{\text{TRAJ}}$  is commonly used as a proxy of  $s_t$ . All these constitute a metric space of observations where distance is defined. Both  $e_t^{\text{OBS}}$  and  $e_t^{\text{TRAJ}}$  are computed by a discriminative forward model, detailed in Section 3.3.

Noteworthy, our intrinsic rewards are episodic, as they are computed from the observations of a single episode only. Arguably, episodic rewards are usually compatible with lifelong rewards and they can be utilized together, but we focus on the former for simplicity in this work and leave such combination for future studies.

#### 3.3 Learning a Discriminative Model

We train a neural network to extract embeddings  $e_t^{\text{OBS}}$  and  $e_t^{\text{TRAJ}}$  from observations in high-dimensional spaces. Furthermore, to obtain better embeddings suitable for exploration, existing studies adopted auxiliary tasks, where the forward and inverse models are two representatives. We propose an improved auxiliary task suitable for exploration in POMDPs inspired by contrastive learning [Laskin *et al.*, 2020]. Concretely, our proposed model learns the environment’s dynamics and discriminates the genuine from the fake trajectories. Figure 2 illustrates the architecture of our model.

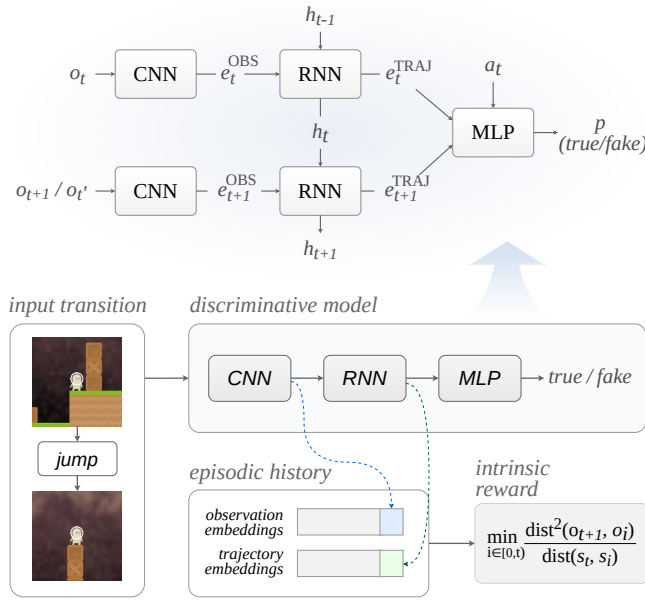


Figure 2: An overview of our proposed DEIR. Given the *input transition* of two observations and an action between them, the *discriminative model* predicts whether they are from a truly observed transition. Observation and trajectory embeddings produced by the model are saved in an *episodic history* to compute *intrinsic rewards* for guiding explorations during RL roll-outs.

### Model Definition

Our discriminative model is denoted as  $\text{Dsc}(o_t, a_t, o_x) : O \times A \times O' \rightarrow [0, 1]$ , where  $o_t, a_t$  are defined above,  $o_x \in \{o_{t+1}, o_{t'}\}$  is either the next observation  $o_{t+1}$  (positive example) or an observation  $o_{t'}$  that is observed recently and randomly selected at time step  $t$  (negative example) for each training sample. In short, the discriminative model estimates the likelihood that the input  $o_x$  is a positive example.

Specifically, to efficiently retrieve fake examples with decent diversity during RL roll-outs, we maintain recent novel observations with a first-in-first-out queue  $\mathbb{Q}$ , so that  $o_{t'}$  can be randomly selected from all observations saved in  $\mathbb{Q}$ . This queue is maintained by keeping adding newly retrieved “novel” observations into it to replace the oldest observations. Here,  $o_t$  is considered “novel” only if  $r_t^I$  is not less than the running average of all intrinsic rewards. Algorithms used in modeling are further detailed in Appendix A.2.

### Proposed Architecture

The proposed intrinsic reward is based on the observation embeddings  $e_t^{OBS}$  and the trajectory embeddings  $e_t^{TRAJ}$  generated by the discriminator. From input to output, the discriminator Dsc is formed by a convolutional neural network (CNN), an recurrent neural network (RNN), and a multi-layer perceptron (MLP) output head. We adopt gated recurrent units (GRU) [Cho *et al.*, 2014] in the RNN module to reduce the number of trainable parameters (compared with LSTM [Hochreiter and Schmidhuber, 1997]). As shown in Figure 2, the CNN takes the observations  $o_t$  and  $o_{t+1}$  as input in parallel and outputs two observation embeddings. Then,

the observation embeddings are fed into the RNN, together with the RNN’s previous hidden state  $h_{t-1}$ . In addition to the updated hidden state  $h_t$ , the RNN outputs the embeddings of two trajectories starting from the beginning of an episode and ending at time step  $t$  and  $t + 1$ , respectively. At last, the two trajectory embeddings with the action  $a_t$  are fed into the MLP for predicting the likelihood. RNN hidden states are saved as part of the discriminative model’s training samples. We adopt Proximal Policy Optimization (PPO) [Schulman *et al.*, 2017], which refreshes its experience buffer more frequently than other algorithms. Therefore we do not apply specialized methods to renew the hidden states within one episode.

### Mini-Batches and Loss Function

During training, each mini-batch consists of two types of samples. Half of them are positive samples, and the other half are negative samples. Both types of samples are picked from the agent’s recent experiences. The discriminator Dsc is trained with a binary cross-entropy loss function [Murphy, 2022] as in ordinary classification tasks.

## 4 Experiments

We answer the following questions through experiments:

- Is DEIR effective in standard benchmark tasks and can it keep performant in hardened, more challenging settings?
- Is our design decision in DEIR generally applicable to a variety of tasks, and particularly, can it generalize to tasks with higher dimensional observations?
- How significantly are each technical component in DEIR contributing to the performance?

### 4.1 Experimental Setup

We evaluate DEIR in two popular procedurally generated RL benchmarks: (1) **MiniGrid** [Chevalier-Boisvert *et al.*, 2018], which is made of 20 grid-world exploration games with different room layouts, interactive objects and goals. An agent needs to learn a specific sequence of actions to reach a final goal with its limited view size. Valid actions include picking up a key, unlocking a door, unpacking a box, and moving an object. No extrinsic reward is available until the goal. (2) **ProcGen** [Cobbe *et al.*, 2020], which consists of 16 games with  $64 \times 64 \times 3$  RGB image inputs, each of which requires a certain level of planning, manipulation or exploration skills to pass. Particularly, each episode is a unique game level, with randomly initialized map settings, physical properties, enemy units and visual objects. Agents need to learn policies that can be generalized to unseen levels.

All environments and network modules are initialized with 20 random seeds in each MiniGrid experiment, and 3 seeds (from the full distribution of game levels) in each ProcGen experiment. All experimental results are reported with the average episodic return of all runs with standard errors. We implement the proposed and the existing exploration methods on top of Proximal Policy Optimization (PPO) [Schulman *et al.*, 2017], which is a widely-used online policy gradient method and has shown decent performance in various RL applications. We conducted hyperparameter search for every

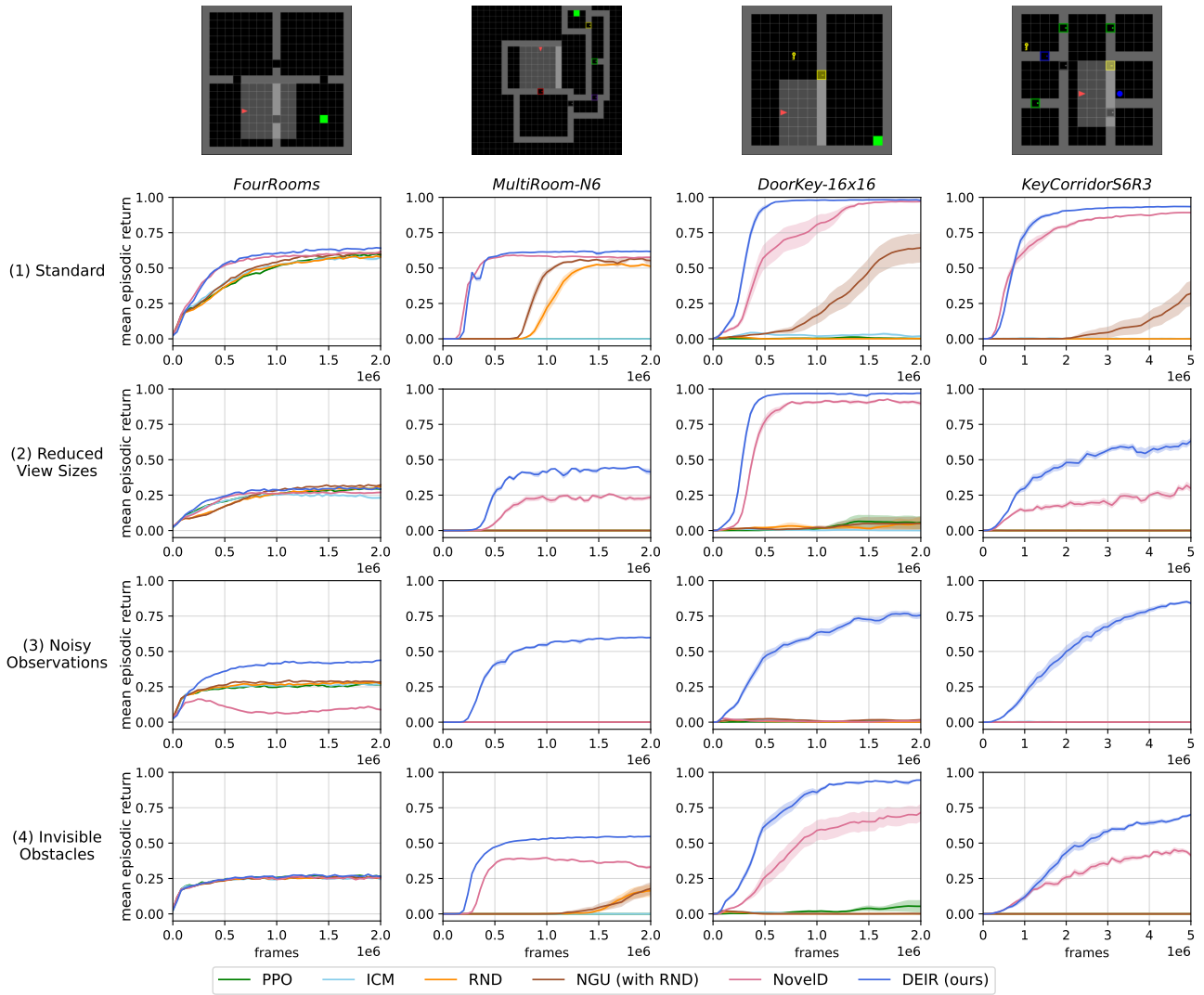


Figure 3: Mean episodic returns in standard (1) and hardened (2-4) MiniGrid games: (1) Agent has a fixed  $7 \times 7$ , unhindered view size. (2) Agent has a reduced view size of  $3 \times 3$  grids. (3) Noisy observations, where Gaussian noise ( $\mu = 0.0, \sigma = 0.1$ ) are added element-wise to the observation that are first normalized to  $[0, 1]$ . (4) Obstacles, invisible to the agent but still in effect. In all figures, Y axes start at -0.05 to show near-zero values.

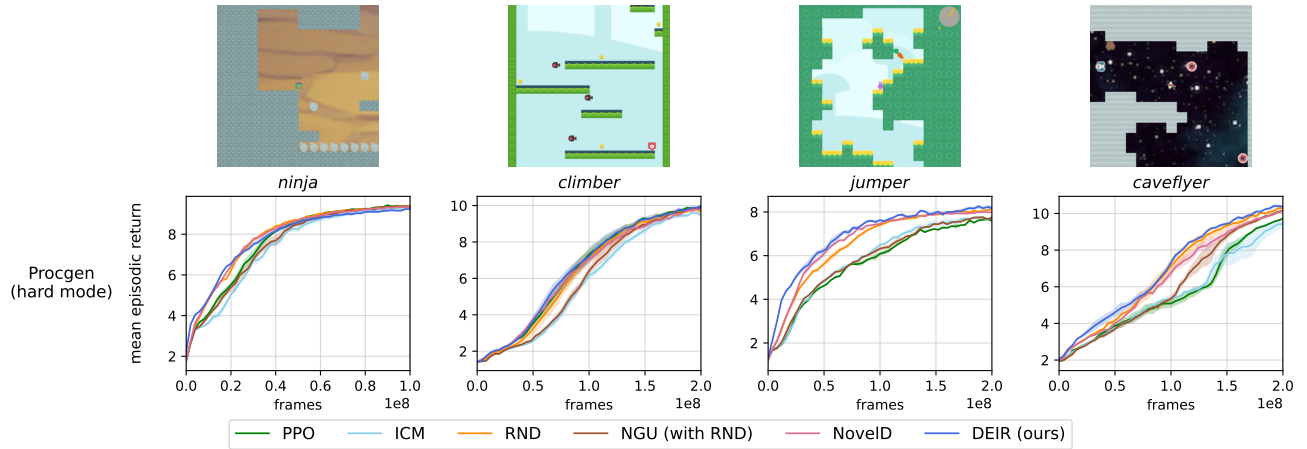


Figure 4: Mean episodic returns in ProcGen (hard mode) games. Episodes are randomly generated from the full distribution of game levels.



method involved in our experiments, to ensure they have the best performance possible. Particularly, we conducted empirical study regarding two key hyperparameters in our proposed method, namely the maximum episode length and maximum observation queue size.

We provide detailed description of benchmark environments, hyperparameters, network structures and computing environments in Appendix A.3 to A.6 respectively.

## 4.2 Evaluation Experiments

### Evaluation in Standard MiniGrid

We first evaluated DEIR’s general performance in four standard MiniGrid tasks, where the agent’s view size is  $7 \times 7$  grids by default and no other constraints are applied. The mean episodic returns of all exploration methods are shown in Figure 3 (first row). In simple tasks *FourRooms* and *MultiRoom-N6*, DEIR and existing methods all presented decent performance. *DoorKey-16x16* and *KeyCorridorS6R3* are more complex tasks, since a successful completion of them needs execution of multiple sub-tasks in a particular order, which requires efficient exploration by the agent. In these complex tasks, DEIR also successfully learned better policies faster.

Furthermore, we compared the performance of DEIR and NovelD in the hardest MiniGrid tasks *ObstructedMaze-Full* (see Figure 5). Its hardness is due to the largest number of sub-tasks required to be completed in the right order among all standards MiniGrid tasks, and only been solved by NovelD so far, albeit requiring excessive time. In contrast, to reach the same SOTA performance, DEIR requires only around 70% time of NovelD, for which we also conducted hyperparameter searches and exceeded its original implementation in requiring fewer training steps.

### Evaluation in Hardened MiniGrid

We further evaluated DEIR’s robustness in 12 MiniGrid tasks with hardened game settings. The following variants were added to the original environment (see examples in Figure 1).

**Reduced view sizes.** The agent’s view size is reduced from the default  $7 \times 7$  grids to the minimal possible view size of  $3 \times 3$  (81.6% reduction in area). Consequently, the agent needs to utilize its observation history effectively.

**Noisy observations.** At each time step, noises sampled from a Gaussian distribution ( $\mu = 0.0, \sigma = 0.1$ ) element-wise and added to the observation that are first normalized to  $[0, 1]$ . With this change, each observation looks novel even if the agent does not explore.

**Invisible obstacles.** Obstacles are invisible to the agent but still in effect: That is, the agent simply perceive them the same way as floors, but cannot step on or pass through them. This requires the agent to have a comprehensive understanding of the environment’s dynamics, beyond the superficial observable novelty.

Results in Figure 3 (second row to fourth row) clearly show that DEIR’s robustness was significantly superior to existing methods in all settings. The performance difference was especially large when only noisy observations were presented. Compared to the results in standard tasks, DEIR lost at most 25% of its returns by the end of the training, while other

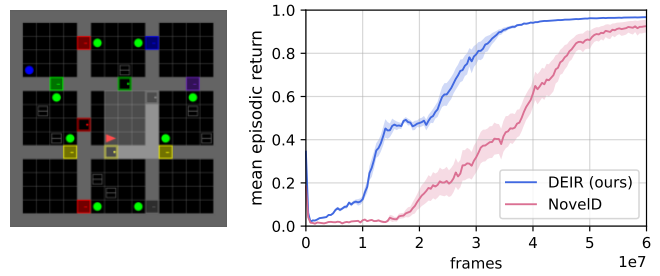


Figure 5: Comparing the mean episodic returns of DEIR and NovelD in *ObstructedMaze-Full* – the hardest standard task in MiniGrid that has only been solved by NovelD so far. DEIR also solves the task but learns significantly faster than NovelD.

methods lost nearly all of their returns in 75% of the noisy-observation tests. Note that our noisy observation is similar to the “noisy-TV” experiments [Burda *et al.*, 2019] but difficult in changing more pixels. In ICM [Pathak *et al.*, 2017], up to 40% of the observation image was replaced with white noise. According to published source code, NovelD was originally tested where at most one special object in an observation switches its color among six hard-coded colors when triggered by the agent, i.e., most part of the observation image remains unchanged. The detailed experimental results in MiniGrid is described in Appendix A.7.

### Generalization Evaluation in ProcGen

We evaluated DEIR’s generalization capability under various reward settings and environmental dynamics in the ProcGen benchmark. Four tasks (on the hard mode) were selected because of their partial observability and demands on exploration skills. We used the same CNN structure as in IMPALA [Espeholt *et al.*, 2018] and Cobbe *et al.*’s work [Cobbe *et al.*, 2020] for the agent’s policy and value function, and a widened version of the CNN used in DQN [Mnih *et al.*, 2015] for the dynamics model of each exploration method. Results in Figure 4 show that DEIR performed better or as well as other exploration methods, while successfully generalized to new game levels generated during training. Also suggested by the results, the proposed model and intrinsic reward are universally applicable to a variety of tasks, including those with higher-dimensional observations. We also confirmed that the performance of DEIR was consistent with the training results reported in previous studies [Cobbe *et al.*, 2020; Cobbe *et al.*, 2021; Raileanu and Fergus, 2021].

## 4.3 Ablation Studies

To better understand DEIR, we created a *KeyCorridorS6R3* task hardened with all three modifications proposed in Section 4.2 (view size: 3, standard deviation of noise: 0.3, with invisible obstacles), and conducted ablation studies to analyze the importance of (1) the conditional mutual information term; (2) the discriminative model;

### Conditional Mutual Information Scaling

To analyze the importance of the conditional mutual information term proposed in Equation 3, we evaluated the performance of our DEIR agent and a variant without the mutual in-

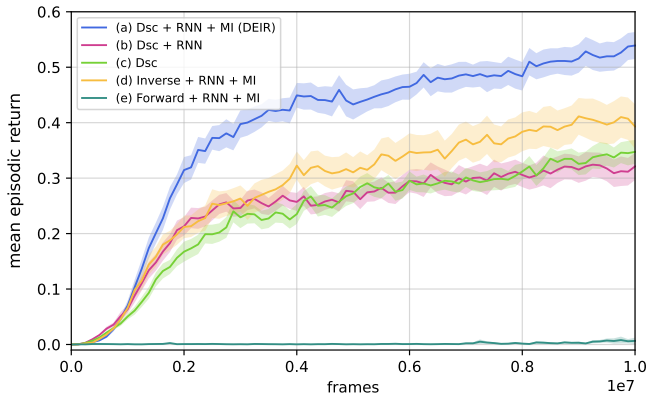


Figure 6: Ablation studies in a hardened *KeyCorridorS6R3* task. The effectiveness of the conditional mutual information (MI) can be confirmed by comparing (a), (b), (c). The difference between (a), (d), (e) shows the discriminator’s importance.

formation scaling term (see Figure 6 (a) and (b)) DEIR’s performance is significantly better than the latter, which proves the importance of our proposed intrinsic reward design.

We use RNN in our model to capture temporal information in trajectories to learn a more accurate representation. Thus we further discuss the effect of RNN on its own. For this purpose, we trained a separate agent with the discriminator only (see Figure 6 (c)), and noticed that using RNN alone barely brings any benefit compared to Figure 6 (b). Thus we are confident that all the performance improvement are indeed contributed by the mutual information scaling term.

#### Discriminative Model

We also show the performance of DEIR agents driven by the inverse model and the forward model (see Figure 6 (d) and (e)). The conditional mutual information term and RNN were applied to all of them, and we used the same tuned hyperparameters in our previous experiments. Compared with Figure 6 (a), our discriminative model-driven agent presented an evident advantage over the agent trained with inverse model alone, while the forward model-driven agent completely failed to learn any meaningful policy in the task (due to the fact that the forward model is notorious for being weak to noise [Pathak *et al.*, 2017]), suggesting that to achieve advanced performance, the discriminative model is indispensable for learning state representations in POMDPs. We believe it is contributed mainly by the trajectory embeddings the discriminative model learns, and we present further analysis results in Section 4.4 for more insights.

#### 4.4 Effectiveness of Learned Embeddings

To get further insights of the impact the learned embeddings on the final performance, we conducted an experiment to compare three model variants. Concretely, we trained a forward-only, an inverse-only and a discriminative model using the same data sampled by a vanilla PPO agent in standard *DoorKey-8x8*, where an agent needs to find a key to open a door that leads to the goal in another room. We devise auxiliary supervised learning tasks, each predicting an important temporal or spatial metric directly related to the

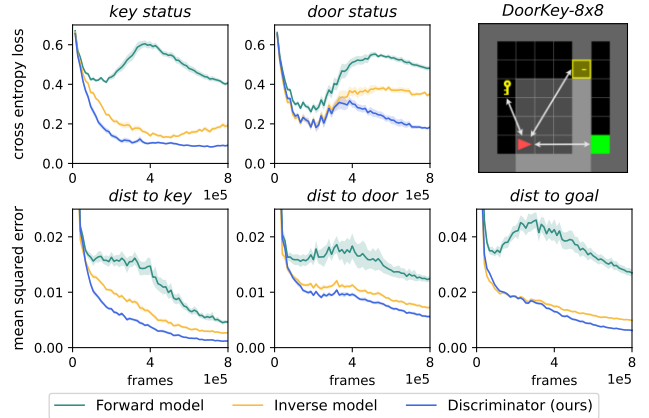


Figure 7: Validation losses of predicting temporal and spatial metrics using trajectory embeddings by three models. Upper-right figure exemplifies the objects (key, door, goal) concerned in metrics. Upper: whether the agent has picked up the key and opened the door. Lower: the agent’s normalized distances to the key, door and goal.

game’s progress or the agent’s position (detailed in Figure 7) given the learned trajectory embeddings  $e^{\text{TRAJ}}$ . Technically, the ground truth metrics are retrieved from the game’s backend, and training stopped after the agent reached a near-optimal policy. Figure 7 demonstrates that our discriminator-based method learns embeddings most helpful in predicting important temporal and spatial metrics, which explains why it benefits downstream objects in RL, including exploration.

In comparison, embeddings from forward and inverse models do not perform as good as ours, which is consistent with the findings in Figure 6. We hypothesize that, the inverse model is less motivated to include historical data in its embeddings, since by design it can reliably infer actions merely from its always-factual inputs. On the other hand, the forward model relies too much on visual details such that its embeddings do not carry much information critical to underlying tasks [Gulrajani *et al.*, 2017; Goyal *et al.*, 2017]

## 5 Conclusions

Training RL agents to explore effectively is a challenging problem, especially in the tasks where rewards are sparse. A promising approach is to augment the extrinsic rewards with novelty-driven intrinsic rewards. However, focusing only on the novelty of observations is insufficient, because an agent may incorrectly recognize the stochasticity in the environment’s dynamics as novelties brought by its explorations. This paper proposes to scale the observation novelty with a conditional mutual information that explicitly relates the agent’s actions to the distances between observations, and to learn a discriminative model that gives better intrinsic rewards. Compared with baselines, our method gives outstanding performance in standard and hardened versions of Mini-Grid, and also demonstrates general applicability to a variety of tasks with higher-dimensional inputs such as those in ProcGen. As future works, we envision researches on exploration in continuous action spaces and multi-agent settings.

## References

- [Agarwal *et al.*, 2021] Rishabh Agarwal, Marlos C Machado, Pablo Samuel Castro, and Marc G Bellemare. Contrastive behavioral similarity embeddings for generalization in reinforcement learning. *arXiv preprint arXiv:2101.05265*, 2021.
- [Andrychowicz *et al.*, 2021] Marcin Andrychowicz, Anton Raichuk, Piotr Stańczyk, Manu Orsini, Sertan Girgin, Raphaël Marinier, Léonard Hussenot, Matthieu Geist, Olivier Pietquin, Marcin Michalski, et al. What matters in on-policy reinforcement learning? a large-scale empirical study. In *International Conference on Learning Representations*, 2021.
- [Ba *et al.*, 2016] Lei Jimmy Ba, Jamie Ryan Kiros, and Geoffrey E. Hinton. Layer normalization. *CoRR*, abs/1607.06450, 2016.
- [Badia *et al.*, 2020] Adrià Puigdomènech Badia, Pablo Sprechmann, Alex Vitvitskyi, Daniel Guo, Bilal Piot, Steven Kapturowski, Olivier Tieleman, Martin Arjovsky, Alexander Pritzel, Andrew Bolt, et al. Never give up: Learning directed exploration strategies. In *International Conference on Learning Representations*, 2020.
- [Baker *et al.*, 2019] Bowen Baker, Ingmar Kanitscheider, Todor Markov, Yi Wu, Glenn Powell, Bob McGrew, and Igor Mordatch. Emergent tool use from multi-agent autotutorials. In *International Conference on Learning Representations*, 2019.
- [Blundell *et al.*, 2016] Charles Blundell, Benigno Uria, Alexander Pritzel, Yazhe Li, Avraham Ruderman, Joel Z Leibo, Jack Rae, Daan Wierstra, and Demis Hassabis. Model-free episodic control. *arXiv preprint arXiv:1606.04460*, 2016.
- [Brockman *et al.*, 2016] Greg Brockman, Vicki Cheung, Ludwig Pettersson, Jonas Schneider, John Schulman, Jie Tang, and Wojciech Zaremba. Openai gym. *CoRR*, abs/1606.01540, 2016.
- [Burda *et al.*, 2019] Yuri Burda, Harrison Edwards, Amos Storkey, and Oleg Klimov. Exploration by random network distillation. In *Seventh International Conference on Learning Representations*, 2019.
- [Chevalier-Boisvert *et al.*, 2018] Maxime Chevalier-Boisvert, Lucas Willems, and Suman Pal. Minimalistic gridworld environment for openai gym. <https://github.com/maximecb/gym-minigrid>, 2018.
- [Cho *et al.*, 2014] Kyunghyun Cho, Bart van Merriënboer, Dzmitry Bahdanau, and Yoshua Bengio. On the properties of neural machine translation: Encoder-decoder approaches. *Syntax, Semantics and Structure in Statistical Translation*, page 103, 2014.
- [Cobbe *et al.*, 2019] Karl Cobbe, Christopher Hesse, Jacob Hilton, and John Schulman. Procgen benchmark. <https://github.com/openai/procgen>, 2019.
- [Cobbe *et al.*, 2020] Karl Cobbe, Chris Hesse, Jacob Hilton, and John Schulman. Leveraging procedural generation to benchmark reinforcement learning. In *International Conference on Machine Learning*, pages 2048–2056. PMLR, 2020.
- [Cobbe *et al.*, 2021] Karl W Cobbe, Jacob Hilton, Oleg Klimov, and John Schulman. Phasic policy gradient. In *International Conference on Machine Learning*, pages 2020–2027. PMLR, 2021.
- [Espeholt *et al.*, 2018] Lasse Espeholt, Hubert Soyer, Remi Munos, Karen Simonyan, Vlad Mnih, Tom Ward, Yotam Doron, Vlad Firoiu, Tim Harley, Iain Dunning, et al. Impala: Scalable distributed deep-rl with importance weighted actor-learner architectures. In *International Conference on Machine Learning*, pages 1407–1416. PMLR, 2018.
- [Goyal *et al.*, 2017] Anirudh Goyal, Alessandro Sordoni, Marc-Alexandre Côté, Nan Rosemary Ke, and Yoshua Bengio. Z-forcing: Training stochastic recurrent networks. In *Advances in neural information processing systems*, volume 30, 2017.
- [Gulrajani *et al.*, 2017] Ishaan Gulrajani, Kundan Kumar, Faruk Ahmed, Adrien Ali Taiga, Francesco Visin, David Vazquez, and Aaron Courville. PixelVAE: A latent variable model for natural images. In *International Conference on Learning Representations*, 2017.
- [Hafner *et al.*, 2020] Danijar Hafner, Timothy Lillicrap, Jimmy Ba, and Mohammad Norouzi. Dream to control: Learning behaviors by latent imagination. In *International Conference on Learning Representations*, 2020.
- [Hochreiter and Schmidhuber, 1997] Sepp Hochreiter and Jürgen Schmidhuber. Long short-term memory. *Neural computation*, 9(8):1735–1780, 1997.
- [Huang *et al.*, 2022] Shengyi Huang, Rousslan Fernand Julien Dossa, Antonin Raffin, Anssi Kanervisto, and Weixun Wang. The 37 implementation details of proximal policy optimization. <https://iclr-blog-track.github.io/2022/03/25/ppo-implementation-details>, 2022.
- [Ioffe and Szegedy, 2015] Sergey Ioffe and Christian Szegedy. Batch normalization: Accelerating deep network training by reducing internal covariate shift. In *International Conference on Machine Learning*, pages 448–456. PMLR, 2015.
- [Laskin *et al.*, 2020] Michael Laskin, Aravind Srinivas, and Pieter Abbeel. Curl: Contrastive unsupervised representations for reinforcement learning. In *International Conference on Machine Learning*, pages 5639–5650. PMLR, 2020.
- [Laurent *et al.*, 2016] César Laurent, Gabriel Pereyra, Philémon Brakel, Ying Zhang, and Yoshua Bengio. Batch normalized recurrent neural networks. In *2016 IEEE International Conference on Acoustics, Speech and Signal Processing (ICASSP)*, pages 2657–2661. IEEE, 2016.
- [Li, 2017] Yuxi Li. Deep reinforcement learning: An overview. *arXiv preprint arXiv:1701.07274*, 2017.



- [Mnih *et al.*, 2015] Volodymyr Mnih, Koray Kavukcuoglu, David Silver, Andrei A Rusu, Joel Veness, Marc G Belle-mare, Alex Graves, Martin Riedmiller, Andreas K Fidjeland, Georg Ostrovski, et al. Human-level control through deep reinforcement learning. *Nature*, 518(7540):529–533, 2015.
- [Murphy, 2022] Kevin P. Murphy. *Probabilistic Machine Learning: An introduction*. MIT Press, 2022.
- [Nair and Hinton, 2010] Vinod Nair and Geoffrey E Hinton. Rectified linear units improve restricted boltzmann machines. In *International Conference on Machine Learning*, pages 807–814, 2010.
- [Pathak *et al.*, 2017] Deepak Pathak, Pulkit Agrawal, Alexei A Efros, and Trevor Darrell. Curiosity-driven exploration by self-supervised prediction. In *International Conference on Machine Learning*, pages 2778–2787. PMLR, 2017.
- [Pritzel *et al.*, 2017] Alexander Pritzel, Benigno Uria, Sri-ram Srinivasan, Adria Puigdomenech Badia, Oriol Vinyals, Demis Hassabis, Daan Wierstra, and Charles Blundell. Neural episodic control. In *International Conference on Machine Learning*, pages 2827–2836. PMLR, 2017.
- [Raffin *et al.*, 2021] Antonin Raffin, Ashley Hill, Adam Gleave, Anssi Kanervisto, Maximilian Ernestus, and Noah Dormann. Stable-baselines3: Reliable reinforcement learning implementations. *Journal of Machine Learning Research*, 22(268):1–8, 2021.
- [Raileanu and Fergus, 2021] Roberta Raileanu and Rob Fergus. Decoupling value and policy for generalization in reinforcement learning. In *International Conference on Machine Learning*, pages 8787–8798. PMLR, 2021.
- [Schulman *et al.*, 2017] John Schulman, Filip Wolski, Prafulla Dhariwal, Alec Radford, and Oleg Klimov. Proximal policy optimization algorithms. *CoRR*, abs/1707.06347, 2017.
- [Sutton and Barto, 2018] Richard S. Sutton and Andrew G. Barto. *Introduction to Reinforcement Learning*. MIT Press, 2nd edition, 2018.
- [Wilmer *et al.*, 2009] EL Wilmer, David A Levin, and Yuval Peres. Markov chains and mixing times. *American Mathematical Soc., Providence*, 2009.
- [Zhang *et al.*, 2021] Tianjun Zhang, Huazhe Xu, Xiaolong Wang, Yi Wu, Kurt Keutzer, Joseph E Gonzalez, and Yuandong Tian. Noveld: A simple yet effective exploration criterion. In *Advances in Neural Information Processing Systems*, 2021.

## A Technical Appendix

Continued from the main text of *DEIR: Efficient and Robust Exploration through Discriminative-Model-Based Episodic Intrinsic Rewards*, the technical appendix consist of the following:

- **A.1 Intrinsic Reward Derivation**, which is referred in Section 3.2.
- **A.2 Algorithms Used in Modeling**, which is referred in Section 3.3.
- **A.3 Benchmark Environments, A.4 Hyperparameters, A.5 Network Structures, A.6 Computing Environments**, which are referred in Section 4.1.
- **A.7 Detailed Experimental Results in MiniGrid**, which is referred in Section 4.2.

### A.1 Intrinsic Reward Derivation

Given a pair of states  $(s_t, s_i), i \in [0, t)$ , a pair of observations  $(o_{t+1}, o_i)$  and the action  $a_t$ , we wish that the policy is optimized with a reward

$$J = \text{dist}(o_{t+1}, o_i) \cdot I(\text{dist}(o_{t+1}, o_i); a_t | s_t, s_i).$$

The first term  $\text{dist}(o_{t+1}, o_i)$  is the distance between observations  $o_{t+1}$  and  $o_i$  as used in previous studies [Badia *et al.*, 2020; Blundell *et al.*, 2016; Pritzel *et al.*, 2017], and the second term  $I(\text{dist}(o_{t+1}, o_i); a_t | s_t, s_i)$  is the conditional mutual information between  $\text{dist}(o_{t+1}, o_i)$  and  $a_t$  given  $s_t, s_i$ . Our intuition behind such design is that the policy achieves novelty by maximizing distance between observations  $(o_{t+1}, o_i)$  and letting the distances to be closely related to  $a_t$ , the action taken in  $s_t$ . This would efficiently eliminate the novelties rooted in transitional uncertainty other than those brought by agent explorations.

Remind that  $I(X; Y|Z) = \mathbb{E}_{p(y,z)} [\text{D}_{\text{KL}}(P(X|Y=y, Z=z) \| P(X|Z=z))]$ . It is because

$$\begin{aligned} I(X; Y|Z) &= \mathbb{E}_{p(x,y,z)} \left[ \log \frac{P(X, Y|Z)}{P(X|Z)P(Y|Z)} \right] \\ &= \mathbb{E}_{p(x,y,z)} \left[ \log \frac{P(X|Y, Z)P(Y|Z)}{P(X|Z)P(Y|Z)} \right] \\ &= \mathbb{E}_{p(y,z)} \left[ \mathbb{E}_{p(x|y,z)} \left[ \log \frac{P(X|Y, Z)}{P(X|Z)} \right] \right] \\ &= \mathbb{E}_{p(y,z)} [\text{D}_{\text{KL}}(P(X|Y=y, Z=z) \| P(X|Z=z))]. \end{aligned}$$

The second term of  $J$  can be expanded as follows (denoting  $D_{t+1,i} \triangleq \text{dist}(o_{t+1}, o_i)$  for simplicity of formulation):

$$\begin{aligned} I(D_{t+1,i}; a_t | s_t, s_i) &= \mathbb{E}_{s_t, s_i, a_t, D_{t+1,i}} [\text{D}_{\text{KL}}(p(D_{t+1,i}, a_t | s_t, s_i) \| p(D_{t+1,i} | s_t, s_i)p(a_t | s_t, s_i))] \\ &= \mathbb{E}_{s_t, s_i, a_t} [\text{D}_{\text{KL}}(p(D_{t+1,i} | a_t, s_t, s_i) \| p(D_{t+1,i} | s_t, s_i))] \end{aligned}$$

We seek to simplify  $J$  which contains an intractable evidence term in the Kullback–Leibler (KL) divergence  $D_{\text{KL}}$ . To do so, we devise a surrogate function for the KL divergence by connecting it with total variation (TV). Denoting  $P(x) = p(x|a_t, s_t, s_i)$  and  $Q(x) = p(x|s_t, s_i)$ , Bretagnolle–Huber inequality gives

$$\begin{aligned} d_{\text{TV}}(P, Q) &\leq \sqrt{1 - \exp(-\text{D}_{\text{KL}}(P \| Q))} \\ \Leftrightarrow \text{D}_{\text{KL}}(P \| Q) &\geq -\log(1 - d_{\text{TV}}^2(P, Q)), \end{aligned}$$

where  $d_{\text{TV}}(P, Q) = \frac{1}{2} \|P - Q\|_1$  is the total variation between  $P$  and  $Q$ . Since  $d_{\text{TV}}(P, Q)$  monotonically increases w.r.t. to KL divergence  $D_{\text{KL}}(P \| Q)$ , we use  $d_{\text{TV}}$  as the surrogate function. Furthermore, given  $a_t, s_t, s_i$  in deterministic environments (including partially observable cases),  $s_{t+1}, o_{t+1}$  and  $D_{t+1,i}$  are uniquely determined.  $P$  can thus be represented as a generalized unit impulse function which has the only non-zero value at  $D_{t+1,i}$ :

$$P(x) = p(x|a_t, s_t, s_i) = \begin{cases} +\infty & x = D_{t+1,i}, \\ 0 & x \neq D_{t+1,i}, \end{cases}$$

$$\int_{\mathcal{D}} P(x) dx = 1,$$

where  $\mathcal{D}$  denotes the set of all possible distances between two observations. Given that property, we further derive the total variation as

$$\begin{aligned}
d_{TV} &= \frac{1}{2} \int_{\mathcal{D}} |P(x) - Q(x)| dx \\
&= \frac{1}{2} \left[ \int_{\mathcal{D}^-} |P(x) - Q(x)| dx + |P(D_{t+1,i}) - Q(D_{t+1,i})| \right] \\
&= \frac{1}{2} \left[ \int_{\mathcal{D}^-} Q(x) dx + |1 - Q(D_{t+1,i})| \right] \\
&= \frac{1}{2} \left[ \int_{\mathcal{D}} Q(x) dx - Q(D_{t+1,i}) + (1 - Q(D_{t+1,i})) \right] \\
&= \frac{1}{2} \times 2 \times (1 - Q(D_{t+1,i})) \\
&= 1 - Q(D_{t+1,i})
\end{aligned}$$

where  $\mathcal{D}^- = \mathcal{D} \setminus \{D_{t+1,i}\}$  denotes the set of all possible distances except  $D_{t+1,i}$ , and by definition of  $Q(x)$ , we have  $\int_{\mathcal{D}} Q(x) dx = 1$  and  $Q(D_{t+1,i}) \leq 1$ . The integrals of  $P$  and  $Q$  can be split and calculated since the number of possible distances involved in RL roll-outs and training is countable [Wilmer *et al.*, 2009].

Now we derive the lower bound of the KL divergence using  $d_{TV}$  :

$$\begin{aligned}
D_{KL}(P||Q) &\geq -\log(1 - d_{TV}^2(P, Q)) \\
&= -\log(1 - (1 - Q(D_{t+1,i}))^2) \\
&= -\log(2 \times Q(D_{t+1,i}) - Q(D_{t+1,i})^2) \\
&\geq -\log(2 \times Q(D_{t+1,i})) \\
&= -\log(2) - \log(Q(D_{t+1,i}))
\end{aligned}$$

where  $-\log(2)$  is constant, and we effectively maximize the last term  $-\log(Q(D_{t+1,i}))$ . As  $D_{t+1,i} \triangleq \text{dist}(o_{t+1}, o_i)$ , which is the (non-negative) distance between two observations  $o_{t+1}, o_i$ , we naturally assume it follows exponential distribution with a mean of the distance of its closest underlying states  $s_t, s_i$ . Setting  $D_{t+1,i}|s_t, s_i \sim \text{Exp}(\lambda = 1/\text{dist}(s_t, s_i))$  with an expected value of  $1/\lambda = \text{dist}(s_t, s_i)$ , we have

$$\begin{aligned}
-\log(Q(D_{t+1,i})) &= -\log(\lambda \exp(-\lambda D_{t+1,i})) \\
&= -\log\left(\frac{1}{\text{dist}(s_t, s_i)} \exp\left(-\frac{\text{dist}(o_{t+1}, o_i)}{\text{dist}(s_t, s_i)}\right)\right) \\
&= \log(\text{dist}(s_t, s_i)) + \frac{\text{dist}(o_{t+1}, o_i)}{\text{dist}(s_t, s_i)}.
\end{aligned}$$

With all that, we can finally define the lower bound of the objective as:

$$J \geq \text{dist}(o_{t+1}, o_i) \times \mathbb{E}_{s_t, s_i, a_i} \left( \log(\text{dist}(s_t, s_i)) + \frac{\text{dist}(o_{t+1}, o_i)}{\text{dist}(s_t, s_i)} \right). \quad (4)$$

Note that alternatively, by keeping only the dominating term  $\text{dist}(o_{t+1}, o_i)/\text{dist}(s_t, s_i)$  and relax expectation to minimum, Equation 4 can be simplified to:

$$J \geq \min_i \frac{\text{dist}^2(o_{t+1}, o_i)}{\text{dist}(s_t, s_i)} \quad (5)$$

which we find is much simpler than, yet performs as well as or even superior to, Equation 4. This is equivalent to the Equation 3 in the main text.

## A.2 Algorithms Used in Modeling

In Algorithm A1, we present the pseudocode for generating the proposed episodic intrinsic reward  $r_t^I$  at time step  $t$  and maintaining the episodic history of observation and trajectory embeddings. In Algorithm A2, the proposed DEIR maintains a queue of recent observations in memory, storing novel observations collected in the most recent episodes. The pseudocode about how DEIR updates the observation queue  $\mathbb{Q}$ , and which kinds of observations are considered “novel” during the updating.

---

### Algorithm A1 Generating intrinsic reward $r_t^I$ at time step $t$

---

**Input:**  $e_t^{\text{OBS}}, E_{\text{OBS}} = \{e_0^{\text{OBS}}, \dots, e_{t-1}^{\text{OBS}}\}$ ,  
 $e_t^{\text{TRAJ}}, E_{\text{TRAJ}} = \{e_0^{\text{TRAJ}}, \dots, e_{t-1}^{\text{TRAJ}}\}$ ,  
 $\text{terminal}(s_t)$

**Output:**  $r_t^I$

- 1: **if**  $E_{\text{OBS}} = \emptyset$  **then**
- 2:     **return** 0
- 3: **end if**
- 4:  $d_{\text{OBS}} \leftarrow$  Euclidean distances between the episodic observation embedding history  $E_{\text{OBS}}$  and  $e_t^{\text{OBS}}$ .
- 5:  $d_{\text{OBS}}^2 \leftarrow$  element-wise squared  $d_{\text{OBS}}$ .
- 6:  $d_{\text{TRAJ}} \leftarrow$  Euclidean distances between the episodic trajectory embedding history  $E_{\text{TRAJ}}$  and  $e_t^{\text{TRAJ}}$ .
- 7:  $d_{\text{JOINT}} \leftarrow d_{\text{OBS}}^2 / d_{\text{TRAJ}}$  (element-wise).
- 8: **if**  $\text{terminal}(s_t)$  **then**
- 9:      $E_{\text{OBS}} \leftarrow \emptyset$
- 10:     $E_{\text{TRAJ}} \leftarrow \emptyset$
- 11: **else**
- 12:     $E_{\text{OBS}} \leftarrow E_{\text{OBS}} \cup e_t^{\text{OBS}}$
- 13:     $E_{\text{TRAJ}} \leftarrow E_{\text{TRAJ}} \cup e_t^{\text{TRAJ}}$
- 14: **end if**
- 15: **return** minimum element in  $d_{\text{JOINT}}$

---



---

### Algorithm A2 Updating the queue of recent observations $\mathbb{Q}$ (from which to randomly select fake training data)

---

**Input:**  $\mathbb{Q}, o_t, r_t^I$ , running average of  $r^I$

**Parameter:** maximum size of  $\mathbb{Q}$ , smoothing factor for updating the running average of intrinsic rewards

**Output:**  $\mathbb{Q}'$

- 1: Update the running average of  $r^I$  with  $r_t^I$ .
- 2: **if**  $\mathbb{Q} = \emptyset$  or  $r_t^I \geq$  the running average of  $r^I$  **then**
- 3:     **if**  $|\mathbb{Q}| =$  maximum size of  $\mathbb{Q}$  **then**
- 4:          $\mathbb{Q}' \leftarrow \mathbb{Q}$  with the oldest element being removed
- 5:          $\mathbb{Q}' \leftarrow \mathbb{Q}' \cup o_t$
- 6:     **else**
- 7:          $\mathbb{Q}' \leftarrow \mathbb{Q} \cup o_t$
- 8:     **end if**
- 9: **end if**
- 10: **return**  $\mathbb{Q}'$

---

In Algorithm A3, Algorithm A4 and Algorithm A5 we describe three types of modifications applied to the environment's observations in hardened MiniGrids games. See Section 4.2 for descriptions about all the three modifications.

---

**Algorithm A3** Processing observations for MiniGrid variants of reduced view sizes

---

**Input:** original  $o_t$  ( $7 \times 7$  view size)

**Output:** processed  $o'_t$  ( $3 \times 3$  view size)

- 1: Let  $(x_{agent}, y_{agent})$  be the fixed coordinates of the agent
  - 2:  $o'_t \leftarrow o_t$  being cropped into a  $3 \times 3$  image centered on  $(x_{agent}, y_{agent} + 1)$  (to always show the agent on the center bottom)
  - 3: **return**  $o'_t$
- 

---

**Algorithm A4** Processing observations for MiniGrid variants of noisy observations

---

**Input:** original  $o_t$ ,  $\mu$ ,  $\sigma$

**Parameter:** the mean and standard deviation of noise

**Output:** processed  $o'_t$

- 1:  $o_{noise} \leftarrow$  Randomly generated image with  $7 \times 7 \times 3$  normally distributed noise (mean:  $\mu$ , standard deviation:  $\sigma$ )
  - 2:  $o'_t \leftarrow o_t + o_{noise}$
  - 3: **return**  $o'_t$
- 

---

**Algorithm A5** Processing observations for MiniGrid variants of invisible obstacles

---

**Input:** original  $o_t$

**Output:** processed  $o'_t$

- 1:  $o'_t \leftarrow o_t$  with all *wall* objects being removed
  - 2:  $o'_t \leftarrow o'_t$  with the colors of *unseen*, *empty* and *wall* grids being changed to the color of the *floor* grid
  - 3: **return**  $o'_t$
-



### A.3 Benchmark Environments

We describe each task environment used in our experiments. More detailed introductions can be found on the official project homepage of each benchmark [Chevalier-Boisvert *et al.*, 2018; Cobbe *et al.*, 2019; Cobbe *et al.*, 2020].

#### Standard MiniGrid Environments

- *FourRooms*: Given four  $8 \times 8$  rooms separated by walls, each room is connected with other two rooms through a  $1 \times 1$  gap in the wall. An agent starts from one room and moves towards the goal in another room. The initial positions of the agent, goal and gaps are randomly selected. This task doesn't include any door or key.
- *MultiRoom-N2-S4*: The task consists of two adjacent rooms to explore. The rooms are connected by a closed but unlocked door. An agent starts from the first room, moving towards the goal in the last room. The maximum size of each room is  $4 \times 4$ . The number of all generated grids is  $25 \times 25$  in total.
- *MultiRoom-N4-S5*: The task consists of four cascaded rooms to explore. Any two adjacent rooms are connected by a closed but unlocked door. An agent starts from the first room, moving towards the goal in the last room. The maximum size of each room is  $5 \times 5$ . The size of all generated grids is  $25 \times 25$ .
- *MultiRoom-N6*: The task is similar to *MultiRoom-N4-S5*, but with six cascaded rooms. The maximum size of each room is  $10 \times 10$ . The size of all generated grids is  $25 \times 25$ .
- *MultiRoom-N30*: A customized *MultiRoom* task, with 30 cascaded rooms. The maximum size of each room is  $10 \times 10$ . The size of all generated grids is  $45 \times 45$ .
- *DoorKey-8x8*: Two adjacent rooms are separated by a wall. An agent needs to find a key in the first room, unlock and open a door in the wall, and reach the goal in the second room. The total size of the two rooms is  $8 \times 8$ . The initial positions of the agent, key, wall, and door are randomly generated. The goal is fixed at the bottom right of the second room.
- *DoorKey-16x16*: The task is similar to *DoorKey-8x8*, but with a total size of  $16 \times 16$ .
- *KeyCorridorS4R3*: The task consists of a corridor and four rooms divided by walls and doors. An agent starting from the corridor in the center needs to find a key from an unlocked room and get to the goal hidden behind another locked door.
- *KeyCorridorS6R3*: The task setting is similar to *KeyCorridorS4R3*, but with six rooms to explore in total.
- *ObstructedMaze-Full*: The task consists of  $3 \times 3$  rooms, each of which is connected by two or more doors and may have multiple interactable objects inside. A ball in a random color is placed in one of the four corner rooms. The agent is required to pick up the ball as its target. To do so, it needs to open locked doors using keys hidden in boxes, and move away balls set in front of doors as obstacles when necessary.

#### Hardened MiniGrid Environments

We show the pseudocode for processing observations in the three hardened MiniGrid variants of reduced view sizes, noisy observations and invisible obstacles in Algorithm A3, A4 and A5, respectively. Note that the agent's view size can be specified as an option when registering the environment in MiniGrid, so we didn't re-implement the resizing function. The pseudocode shown in A3 is mainly for a better description.

#### ProcGen Environments

- *Ninja*: A side-scroller game with multiple narrow ledges randomly placed at different horizontal levels. The agent starting from the leftmost needs to jump across those ledges and get to the goal placed on the top of a ledge on the right. When moving towards the goal, the agent must either avoid bomb obstacles or destroy them by attacks. Taking "jump" actions over multiple timesteps can let the agent jump higher. The maximum reward is 10 for reaching the goal.
- *Climber*: A vertical platform game. The agent starts at the bottom of the screen, and needs to climb a number of platforms to get to the top while collecting as many stars as possible along the way. The agent can get a small reward by collecting a star, and get a larger reward after collecting all stars in an episode. An episode ends after all stars are collected or the agent is caught by flying monsters scattered throughout the game.
- *Jumper*: An open-world game with an agent, a goal, obstructive terrains, and stationary enemies. All objects in the world are completely randomly placed. The agent may need to ascend or descend its horizontal level and avoid obstacles and enemies by jumping. The agent is also capable of "double jumping", namely, it can jump the second time while in the air. A reward of 10 is given after reaching the goal.
- *Caveflyer*: An open-world game, in which the agent needs to explore multiple connected caves to find an exit (the goal). The agent can rotate and move forward or backward, as in a physical environment with both velocity and acceleration. In addition to obstructive terrains, there might also be moving enemies and bonus targets. The agent can get extra rewards by destroying bonus targets (3 points per target) and a fixed completion reward of 10 for reaching the goal.

Each ProcGen task has an option to specify the difficulty of levels to generate. We conducted all experiments on the hard mode. Compared with easy mode games, hard mode games are larger in size and have more obstacles and enemies, and thus are harder for the agent to obtain rewards.

## A.4 Hyperparameters

Hyperparameters used for training each method in MiniGrid and ProcGen environments are summarized in Table A1.

### Hyperparameter Selection

In the experiments, all methods are implemented on top of PPO. Therefore, the hyperparameters of PPO were shared among all methods while the hyperparameters of each method, including intrinsic reward coefficient were tuned separately. Hyperparameters were initially searched in *DoorKey-8x8* and *Jumper* tasks for MiniGrid and ProcGen experiments, and then partially adjusted per the results in *DoorKey-16x16*, *KeyCorridorS6R3*, *ObstructedMaze-Full (OMFull)* and *Caveflyer* tasks. The values that consistently performed well across all tests were selected, and used in the experiments. For methods that failed to learn any effective policy in difficult tasks, we selected hyperparameters for them according to their best records in simpler tasks.

### Normalization for Hidden Layers

We applied batch normalization [Ioffe and Szegedy, 2015] to all non-RNN hidden layers used in MiniGrid experiments (except for *OMFull*), and applied layer normalization [Ba *et al.*, 2016] to all CNN layers in ProcGen experiments (and in *OMFull*). It is because that in tasks with stable observation distributions, we found that applying batch normalization to all non-RNN layers could significantly boost up the learning speed. Similar results were also observed when applying batch normalization to RNN layers. However, we only adopted batch normalization for non-RNN layers in order to avoid the risk of causing serious overfitting [Laurent *et al.*, 2016]. In tasks with ever-changing observations like ProcGen games, we applied layer normalization to all CNN layers, together with a smaller learning rate to learn policies in a more gradual way.

### Normalization for Intrinsic Rewards

Following RND and NGU, we normalized intrinsic rewards for all methods using the formula  $(r_t^I - \mu_{IR})/\sigma_{IR}$ , where  $\mu_{IR}$  and  $\sigma_{IR}$  are respectively the exponential moving average and standard deviation of intrinsic rewards.  $\mu_{IR}$  and  $\sigma_{IR}$  were updated using all samples collected in one RL roll-out, and the momentum values for old  $\mu_{IR}$  and  $\sigma_{IR}$  were set as 0.9 except for NGU. It was because NGU already normalized the squared Euclidean distances when generating intrinsic rewards.

### Normalization for Advantages

In MiniGrid experiments, we found advantage normalization [Huang *et al.*, 2022; Andrychowicz *et al.*, 2021] was helpful in improving both learning speed and exploration efficiency, and we applied it in all MiniGrid experiments. The momentum for computing exponential moving averages and standard deviations was 0.9. In ProcGen experiments, we also found that advantage normalization could facilitate early exploration, but the agent’s policy was occasionally trapped in local optima when it was enabled. Since this problem was not observed in MiniGrid, we applied advantage normalization in MiniGrid only.

### Maximum Episode Length

For the experiments reported in the main paper and in Figures A3, A4 and A5, we simply used the default maximum episode length set by the benchmark and observed that DEIR outperforms other methods in most tasks. We additionally evaluated whether DEIR can perform well with other maximum episode lengths, as an episodic exploration method. We compared its performance in *MultiRoom-N30* environments with maximum episode lengths of 300, 500, 1000, 2000, and 5000. (The default maximum episode length is the number of rooms  $\times 20$  in standard *MultiRoom* games, and thus is 600 in *MultiRoom-N30*.) Besides the fixed completion reward of 1.0, the original MiniGrid environment also gives a time penalty to encourage completing the game using fewer steps. The time penalty is computed based on the ratio of used steps and maximum steps, and thus may be affected when changing the maximum episode length. For fair comparisons, we temporarily disabled the time penalty from the environment.

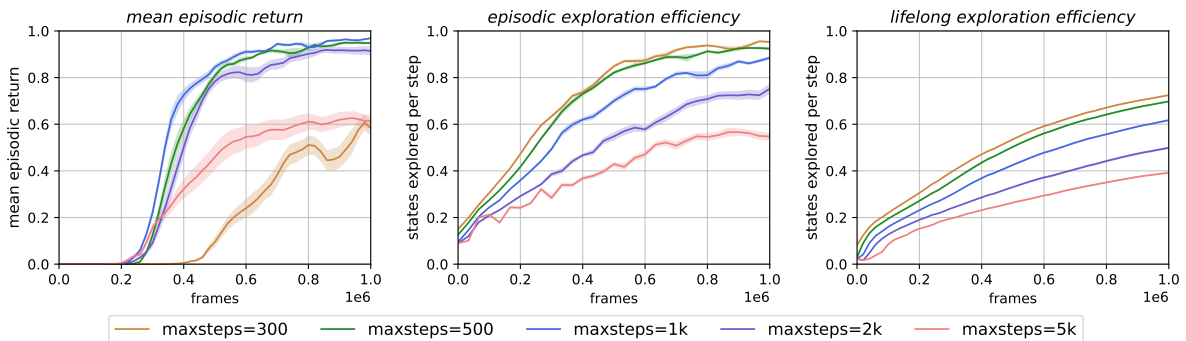


Figure A1: Results on maximum episode length. In the *MultiRoom-N30* environment, DEIR performs well with a relatively wide range of maximum episode lengths (e.g., 500, 1000 and 2000). Too short lengths (e.g., 300) may cause the agent to be less likely to reach the goal and thus focus only on obtaining intrinsic rewards. Too long lengths (e.g., 5000) may prevent the agent from collecting sufficient intrinsic rewards in later steps of the episode.

Hyperparameter	MiniGrid	OMFull (*)	ProcGen	Candidate Values
PPO $\gamma$	0.99	0.99	0.99	0.99, 0.997, 0.999
PPO $\lambda_{\text{GAE}}$	0.95	0.95	0.95	0.0, 0.8, 0.9, 0.95, 0.99, 0.997
PPO rollout steps	512	256	256	128, 256, 512, 1024, 2048, 4096
PPO workers	16	64	64	16, 32, 64, 128
PPO clip range	0.2	0.2	0.2	0.1, 0.2, 0.3
PPO training epochs	4	3	3	2, 3, 4
model training epochs	4	3	3	1, 3, 4
mini-batch size	512	2048	2048	512, 1024, 2048
entropy loss coef	$1 \times 10^{-2}$	$5 \times 10^{-4}$	$1 \times 10^{-2}$	$5 \times 10^{-4}$ , $1 \times 10^{-3}$ , $1 \times 10^{-2}$ , $1 \times 10^{-1}$
advantage normalization	yes	no	no	yes, no
adv norm momentum	0.9	-	-	0.0, 0.9, 0.95, 0.99, 0.999
Adam learning rate	$3 \times 10^{-4}$	$1 \times 10^{-4}$	$1 \times 10^{-4}$	$3 \times 10^{-5}$ , $1 \times 10^{-4}$ , $3 \times 10^{-4}$ , $1 \times 10^{-3}$
Adam epsilon	$1 \times 10^{-5}$	$1 \times 10^{-5}$	$1 \times 10^{-5}$	$1 \times 10^{-2}$ , $1 \times 10^{-4}$ , $1 \times 10^{-5}$ , $1 \times 10^{-8}$
Adam beta1	0.9	0.9	0.9	0.9, 0.95, 0.99
Adam beta2	0.999	0.999	0.999	0.999, 0.9999
normalization for layers	Batch Norm	Layer Norm	Layer Norm	Batch Norm, Layer Norm, no
seeds in experiments	20	12	3	(decided per our computing capabilities)
extrinsic reward coef	1.0	10.0	1.0	
<i>DEIR</i>				
IR (intrinsic reward) coef $\beta$	$1 \times 10^{-2}$	$1 \times 10^{-3}$	$5 \times 10^{-2}$ (**)	$1 \times 10^{-3}$ , $3 \times 10^{-3}$ , $5 \times 10^{-3}$ , $1 \times 10^{-2}$ , $3 \times 10^{-2}$ , $5 \times 10^{-2}$ , $1 \times 10^{-1}$
IR normalization	yes	yes	yes	yes, no
IR norm momentum	0.9	0.9	0.9	0.0, 0.9, 0.95, 0.99, total average
observation queue size	$1 \times 10^5$	$1 \times 10^5$	$1 \times 10^5$	$1 \times 10^4$ , $1 \times 10^5$ , $1 \times 10^6$
<i>NovelD</i>				
IR coefficient $\beta$	$3 \times 10^{-2}$	$3 \times 10^{-3}$	$3 \times 10^{-2}$	$1 \times 10^{-4}$ , $1 \times 10^{-3}$ , $3 \times 10^{-3}$ , $5 \times 10^{-3}$ , $1 \times 10^{-2}$ , $3 \times 10^{-2}$ , $5 \times 10^{-2}$ , $1 \times 10^{-1}$
IR normalization	yes	yes	yes	yes
IR norm momentum	0.9	0.9	0.9	0.9
RND error normalization	no	no	no	yes, no (using IR norm only performed better)
RND error momentum	total avg	total avg	total avg	0.997, total average
<i>NGU</i>				
IR coefficient $\beta$	$1 \times 10^{-3}$	-	$3 \times 10^{-4}$	$1 \times 10^{-4}$ , $3 \times 10^{-4}$ , $1 \times 10^{-3}$ , $3 \times 10^{-3}$ , $5 \times 10^{-3}$ , $1 \times 10^{-2}$ , $3 \times 10^{-2}$ , $1 \times 10^{-1}$
IR normalization	yes	-	yes	yes, no
IR norm momentum	0.0	-	0.0	0.0, 0.2, 0.5, 0.9
RND-based lifelong bonus	yes	-	yes	yes, no
RND error normalization	yes	-	yes	yes, no
RND error momentum	total avg	-	total avg	0.997, total average
momentum (squared dist.)	0.997	-	0.997	0.99, 0.997, 0.999, 0.9999, total average
<i>RND</i>				
IR coefficient $\beta$	$3 \times 10^{-3}$	-	$1 \times 10^{-2}$	$1 \times 10^{-5}$ , $1 \times 10^{-4}$ , $1 \times 10^{-3}$ , $3 \times 10^{-3}$ , $5 \times 10^{-3}$ , $1 \times 10^{-2}$ , $3 \times 10^{-2}$
IR normalization	yes	-	yes	yes, no
IR norm momentum	0.9	-	0.9	0.0, 0.9
RND error normalization	no	-	no	yes, no (using IR norm only performed better)
RND error momentum	total avg	-	total avg	0.997, total average
<i>ICM</i>				
IR coefficient $\beta$	$1 \times 10^{-2}$	-	$1 \times 10^{-4}$	$3 \times 10^{-5}$ , $1 \times 10^{-4}$ , $3 \times 10^{-4}$ , $1 \times 10^{-3}$ , $3 \times 10^{-3}$ , $5 \times 10^{-3}$ , $1 \times 10^{-2}$ , $3 \times 10^{-2}$
IR normalization	yes	-	yes	yes
IR norm momentum	0.9	-	0.9	0.9
forward loss coef.	0.2	-	0.2	0.2 (following the original paper)

Table A1: Hyperparameters used for training each method in MiniGrid and ProcGen. Hyperparameters were searched in *DoorKey-8x8* and *Junper*, and partially adjusted according to results in *DoorKey-16x16*, *KeyCorridorS6R3*, *ObstructedMaze-Full* and *Caveflyer* tasks. Values performed best across all tests were selected and used in the remaining experiments. The term “momentum” refers to the smoothing factor in the exponential moving average (EMA) used to calculate the running mean and variance. The listed values contain all values that have been searched and tested in at least one experiment. Due to limited computing resources, we only search a subset of all possible combinations of the listed parameter values. (\*) OMFull refers to *ObstructedMaze-Full* in MiniGrid, \*\* DEIR uses  $\beta = 5 \times 10^{-3}$  in *Caveflyer*

The results in Figure A1 demonstrate that DEIR can perform robustly within a wide range of maximum episode lengths, at least ranging from 500 to 2000 and covering the default maximum length of 600. Also, we believe DEIR can perform even better if the maximum episode length is specifically optimized or dynamically managed.

### Maximum Observation Queue Size

Another hyperparameter included in our proposal of DEIR is the maximum length of the first-in-first-out queue  $\mathbb{Q}$  – as described in Section 3.3 and Algorithm A2,  $\mathbb{Q}$  stores recent novel observations to make fake input data for the discriminative model’s training. In order to make clear the most suitable value for it, we conducted experiments on different maximum sizes for  $\mathbb{Q}$ .

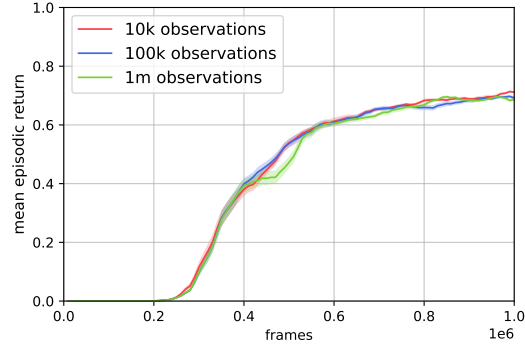


Figure A2: Comparing mean episodic returns when using different maximum sizes for the recent observation queue  $\mathbb{Q}$ . Results show that DEIR is compatible with a wide range of observation queue sizes, ranging from  $1 \times 10^4$  to  $1 \times 10^6$ .

Results shown in Figure A2 suggest that, in the *MultiRoom-N30* environment, DEIR can actually work well with a wide range of observation queue sizes, ranging from  $1 \times 10^4$  to  $1 \times 10^6$ . Nonetheless, in order to save computing resources while keeping better diversity, we adopted  $1 \times 10^5$  in the main experiments.

## A.5 Network Structures

We define the structures of policy and value networks, and the proposed discriminative model, which were updated separately in parallel to the training of PPO agents. Policy and value networks shared the same CNN and RNN modules, but used separate MLP output heads. Specifically for CNNs: In MiniGrid experiments, we used the CNN structure simplified from the CNN used in DQN [Mnih *et al.*, 2015] for both the policy and the model. In ProcGen experiments, we used the same CNN structure as in IMPALA [Espeholt *et al.*, 2018] and Cobbe *et al.*’s work [Cobbe *et al.*, 2020] for the agent’s policy and value function, and a widened version of the CNN used in DQN for the dynamics model.

### Policy and value networks (MiniGrid)

#### CNN (view size $7 \times 7$ )

Conv2d(in=3, out=32, kernel=2, stride=1, pad=0),  
Conv2d(in=32, out=64, kernel=2, stride=1, pad=0),  
Conv2d(in=64, out=64, kernel=2, stride=1, pad=0),  
FC(in=1024, out=64).

#### CNN (view size $3 \times 3$ )

Conv2d(in=3, out=32, kernel=2, stride=1, pad=1),  
Conv2d(in=32, out=64, kernel=2, stride=1, pad=0),  
Conv2d(in=64, out=64, kernel=2, stride=1, pad=0),  
FC(in=256, out=64).

#### RNN

GRU(in=64, out=64).

#### MLP (value network)

FC(in=64, out=128),  
FC(in=128, out=1).

#### MLP (policy network)

FC(in=64, out=128),  
FC(in=128, out=number of actions).

*FC* stands for the fully connected linear layer, and *Conv2d* refers to the 2-dimensional convolutional layer, *GRU* is the gated recurrent units [Cho *et al.*, 2014]. In MiniGrid games, batch normalization and ReLU [Nair and Hinton, 2010] are applied after each hidden layer listed above, except for the layers inside the RNN modules. Batch normalization is also used for normalizing input images.

### Discriminative model (MiniGrid)

**CNN** Same structure as the policy and value networks.

**RNN** Same structure as the policy and value networks.

#### MLP

FC(in= $64 \times 2 + \text{number of actions}$ , out=128),  
FC(in=128, out=128),  
FC(in=128, out=1).

Batch normalization and ReLU are applied after each hidden layer, except for RNN layers. Batch normalization is also applied to input images.

### Policy and value networks (Procegn)

#### CNN

Same structure as the CNN used in IMPALA,  
FC(in=2048, out=256).

#### RNN

GRU(in=256, out=256).

#### MLP (value network)

FC(in=256, out=256),  
FC(in=256, out=1).

#### MLP (policy network)

FC(in=256, out=256),  
FC(in=256, out=number of actions).

In ProcGen games (and *ObstructedMaze-Full* in MiniGrid), layer normalization and ReLU are applied after each CNN layer. Layer normalization is also used for input images.



### **Discriminative model (ProcGen)**

#### **CNN**

Conv2d(in=3, out=32, kernel=8, stride=4, pad=0),  
Conv2d(in=32, out=64, kernel=4, stride=2, pad=0),  
Conv2d(in=64, out=64, kernel=4, stride=1, pad=0),  
FC(in=576, out=256).

#### **RNN**

GRU(in=256, out=256).

#### **MLP**

FC(in=256  $\times$  2 + number of actions, out=256),  
FC(in=256, out=256),  
FC(in=256, out=1).

Layer normalization and ReLU are applied after each CNN layer. Layer normalization is also used for input images.

### **Implementations of Other Methods**

For fair comparisons, we basically adopted the same model structure as the discriminative model for the networks of existing exploration methods used in our experiments, except for RND and RND-based methods. In RND, NovelD and NGU, the MLP heads of the target and predictor networks were larger than those in other methods, in order to alleviate the problem of vanishing lifelong rewards.

For ICM, RND, and NovelD, we reproduced those methods based on their original papers and open-source code, but adopted newly-tuned hyperparameters and network structures when applicable.

For NGU, the NGU method in our experiments is not entirely identical to the original implementation. It is because the learning framework we adopted for training and comparing all exploration methods is more lightweight than the originally proposed one. However, we confirmed that every step of the original algorithm for intrinsic reward generation was followed in our reproduction (according to the original definition given in NGU’s paper).

Our PPO agents were created based on the implementation of PPO in Stable Baselines 3 (1.1.0 version) [Raffin *et al.*, 2021].

For more details on our implementation of existing methods, please refer to our source code (to be released after publication).

## A.6 Computing Environments

All experiments were done on six compute nodes with the following hardwares and softwares.

- CPU: AMD Ryzen Threadripper 1950X, 2990WX.
- GPU: NVIDIA GeForce GTX 1080 Ti, 2 GPUs per node.
- Memory: 128 GB per node.
- OS: Linux-5.4.0-122-generic-x86\_64-with-glibc2.31.
- Python version: 3.9.7.
- numpy version: 1.22.3.
- stable-baselines3 version: 1.1.0 [Raffin *et al.*, 2021].
- gym version: 0.23.1 [Brockman *et al.*, 2016].
- gym-minigrid version: 1.0.2 [Chevalier-Boisvert *et al.*, 2018].
- ProcGen version: 0.10.7 [Cobbe *et al.*, 2020].

## A.7 Detailed Experimental Results in MiniGrid

In addition to the experimental results reported in the main paper, we show the full results in MiniGrid games with Figures A3, A4 and A5. Particularly, besides mean episodic returns as the main performance metric, we used the below two metrics for evaluating the exploration efficiency of each method.

- **Episodic exploration efficiency:** the number of states explored per timestep that have never been seen in the current episode.
- **Lifelong exploration efficiency:** the number of states explored per timestep that have never been seen across all previous episodes.

Full state information is directly acquired from the backend of MiniGrid games for evaluation and analysis only. We noticed that the values of states are not equal. An agent may only explore a smaller number of unique states, while those states are actually more valuable overall. However, considering that there is no ground truth available for measuring the absolute value of a state, the two metrics defined above can be used to estimate the exploration efficiency of a method in an objective and relatively accurate way.

The experimental results on exploration efficiency in Figures A4 and A5 further clearly suggest that the proposed DEIR can explore more efficiently and robustly than other methods in both standard and hardened MiniGrid environments.

Mean Episodic Returns in MiniGrid

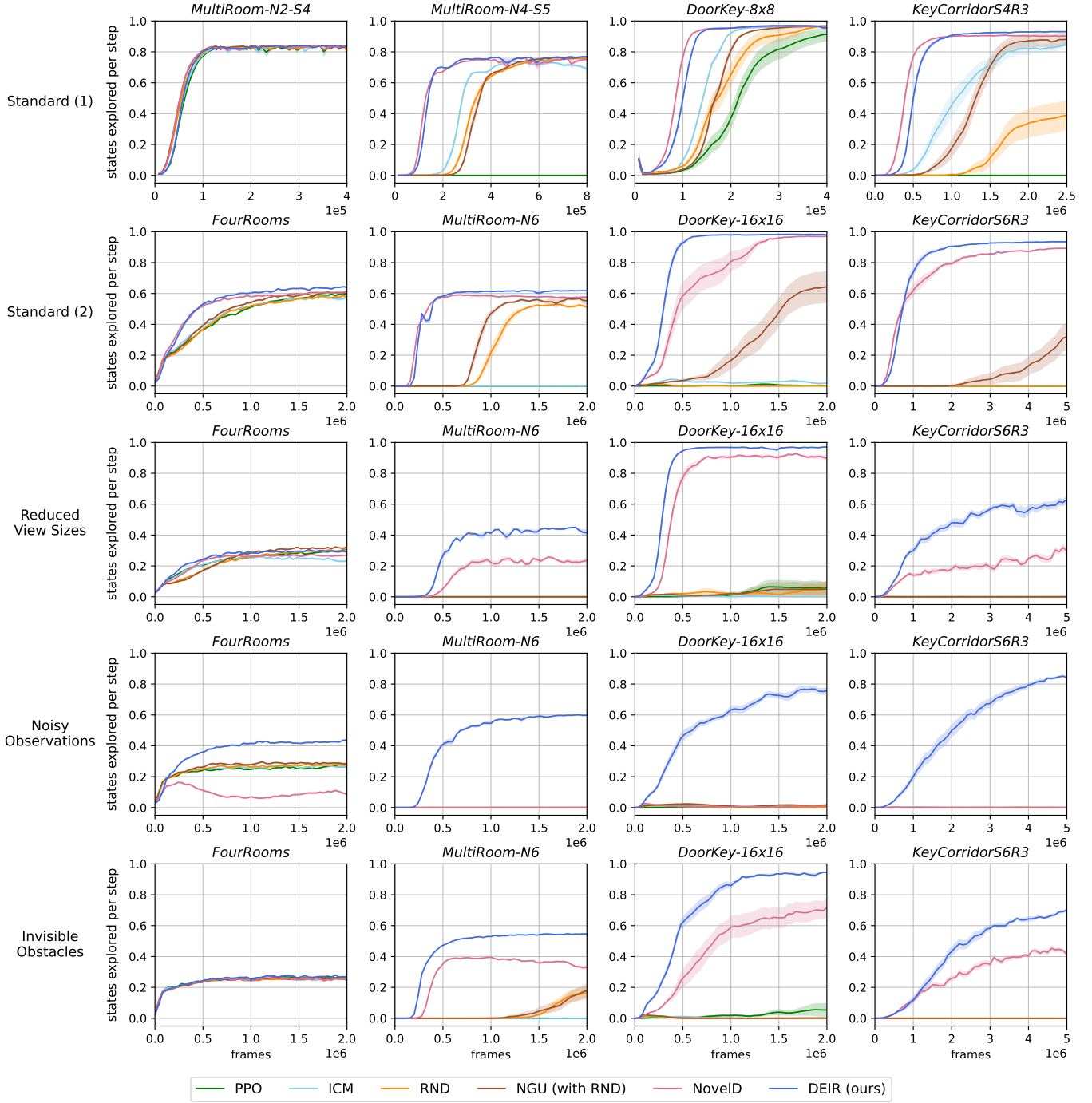


Figure A3: Full results of **mean episodic returns** in standard and hardened MiniGrid games. Standard tasks shown in the first row are small in size, consisting of fewer grids in total, and thus are easier than tasks shown in the second row.

Episodic Exploration Efficiency in MiniGrid

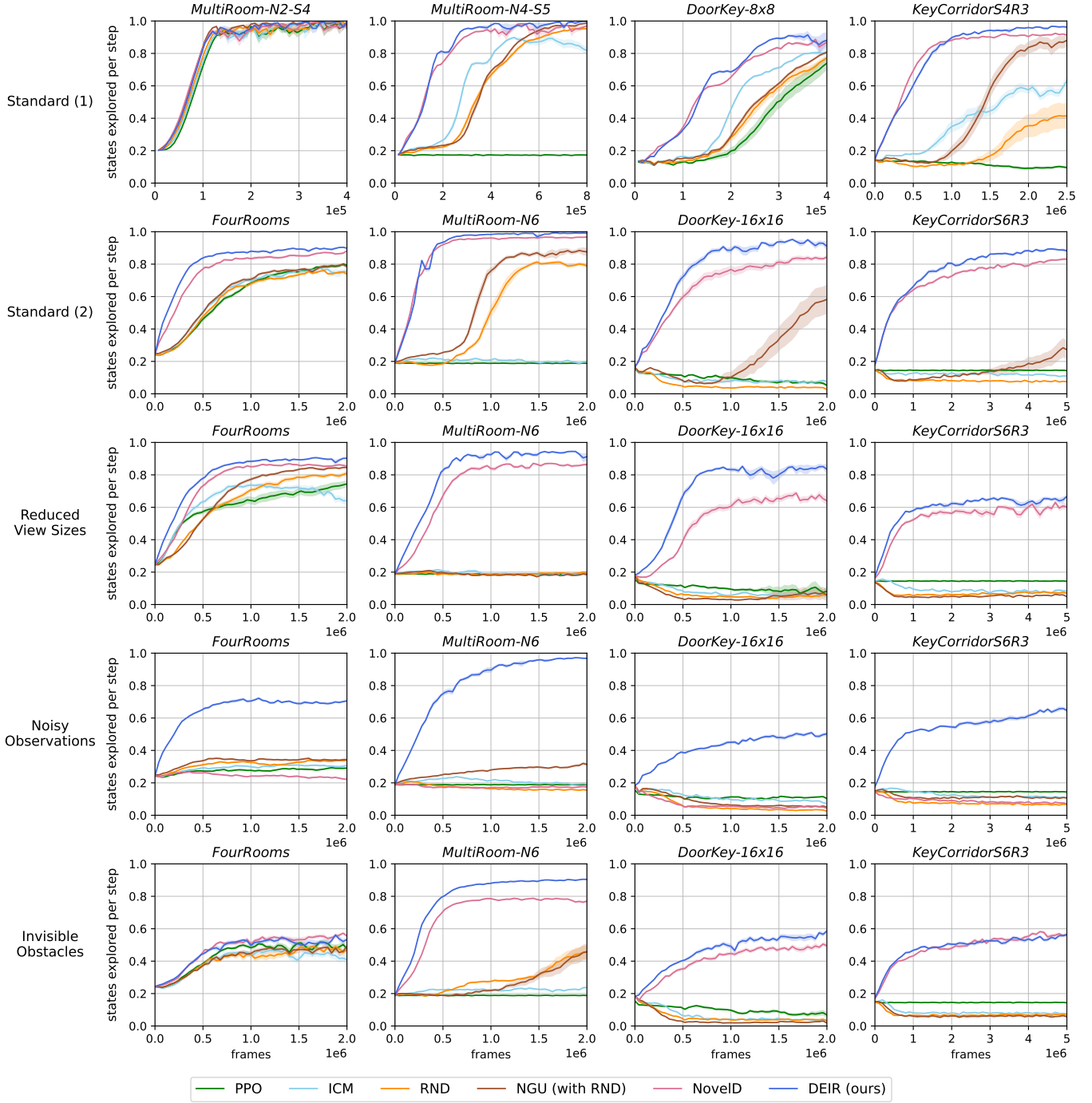


Figure A4: Full results of **episodic exploration efficiency** in standard and hardened MiniGrid games. Standard tasks shown in the first row are small in size, consisting of fewer grids in total, and thus are easier than tasks shown in the second row.



Lifelong Exploration Efficiency in MiniGrid

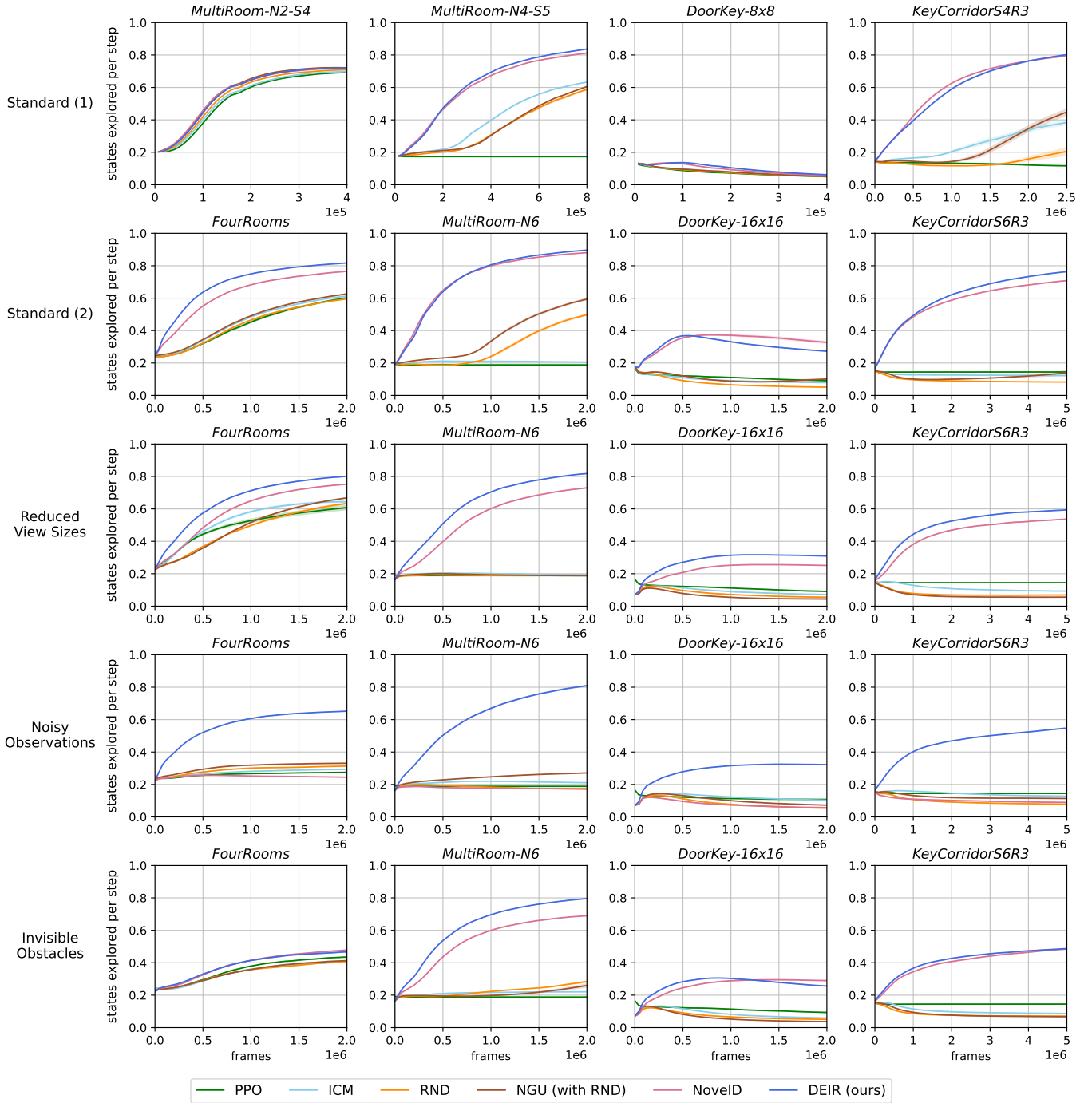


Figure A5: Full results of **lifelong exploration efficiency** in standard and hardened MiniGrid games. Standard tasks shown in the first row are small in size, consisting of fewer grids in total, and thus are easier than tasks shown in the second row.